Compression Failure of Quasibrittle Material: Nonlocal Microplane Model

By Zdeněk P. Bažant,[1] Fellow, ASCE, and Joško Ožbolt[2]

Abstract: The previously presented constitutive model of microplane type for nonlinear triaxial behavior and fracture of concrete is used in nonlocal finite element analysis of compression failure in plane strain rectangular specimens. For specimens with sliding rigid platens there is a bifurcation of the loading path at the beginning of postpeak softening; a symmetric (primary) path exists but the actual (stable) path is the nonsymmetric (secondary) path, involving an inclined shear-expansion band that consists of axial splitting cracks and is characterized by transverse expansion. The secondary path is indicated by the first eigenvalue of the tangent stiffness matrix but can be more easily obtained if a slight nonsymmetry is introduced into the finite element model. In specimens with bonded rigid platens there is no bifurcation; they fail symmetrically, by two inclined shear-expansion bands that consist of axial splitting cracks. The transverse expansion produces transverse tension in the adjacent material, which serves as the driving force of propagation of the axial splitting cracks. Numerical calculations indicate no significant size effect on the nominal stress at maximum load.

Introduction

Under uniaxial compression, quasibrittle materials exhibiting progressive distributed damage, such as concrete, rocks, ceramics, and ice, fail by slip on inclined shear bands or by axial splitting, or by a combination of both. From experience, the axial splitting cracks appear to be an important part of the compression failure mechanism in quasibrittle materials. However, although various aspects of the microscopic fracture mechanism under compression have been illustrated in previous works [e.g., Griffith (1924); Kendall (1978); Miyamoto et al. (1977); Sammis and Ashby (1986); Shetty et al. (1968); Ingraffea (1977); Glucklich (1963); Bažant (1967)], no realistic comprehensive model for macroscopic compression failure process has been presented. The reason is that a sufficiently realistic constitutive model applicable to cracking damage under general triaxial stress states, including compressive stress states, has been unavailable, and a method to overcome the spurious mesh sensitivity and localization problems due to triaxial strain softening did not exist. Recently, both of these problems were overcome with the nonlocal version (Bažant and Ožbolt 1990) of the microplane model (Bažant and Prat 1988). The purpose of this paper is to apply this model to study the compression failure.

Compression failure of uniaxial concrete test specimens was recently analyzed by a nonlocal finite element code in Droz and Bažant (1988) [see also Bažant (1989a)]. The analysis indicated a shear-band mode of failure, but the axial splitting often seen in experiments could not be obtained. However, the constitutive model used, namely Drucker-Prager plasticity with a nonlocal degrading yield limit, was not sufficiently realistic for con-

[1]Walter P. Murphy Prof. of Civ. Engrg., Northwestern Univ., Evanston, IL 60208.
[2]Res. Engr., Institut für Werkstoffe im Bauwesen, Universität Stuttgart, Germany; formerly, Visiting Scholar, Northwestern Univ.

Note. Discussion open until August 1, 1992. To extend the closing date one month, a written request must be filed with the ASCE Manager of Journals. The manuscript for this paper was submitted for review and possible publication on February 27, 1991. This paper is part of the *Journal of Engineering Mechanics*, Vol. 118, No. 3, March, 1992. ©ASCE, ISSN 0733-9399/92/0003-0540/$1.00 + $.15 per page. Paper No. 1469.

crete. A nonlocal finite element approach based on a more realistic constitutive model for concrete was formulated in a preceding paper by Bažant and Ožbolt (1990). The present paper will apply this model to the study of compression failure. All the definitions and notations from the preceding paper are retained and the basic mathematical formulation is not repeated.

Axial Splitting Fracture

Axial splitting due to compression is a difficult problem in fracture mechanics, which has a long history. The difficulty arises principally due to the fact that, in uniaxially compressed specimens whose macroscopic strain field is uniform, calculation yields no release of stored elastic energy into a propagating axial fracture, that is, the driving force of fracture propagation is lacking. The reason is that, if a planar crack parallel to the compression direction is introduced into a uniaxial compressive stress field, there is no change in stress since the stresses on the crack planes are zero to begin with. Therefore, some mechanism that breaks the macroscopic uniformity of the strain field must exist.

One hypothesis, which was explored in some detail, was that transverse tensions are created due to three-dimensional buckling [e.g., Bažant (1967)]. From second-order three-dimensional buckling analysis with finite strains (reviewed in Bažant and Cedolin (1991), section 11.7), however, it transpired that three-dimensional buckling could have a significant effect only if the axial normal compressive stress reached approximately the same order of magnitude as the tangential transverse modulus (stiffness) or the tangential shear modulus of the material. This is possible only for highly anisotropic materials such as fiber composites or laminates, for which the three-dimensional buckling hypothesis had some success in explaining certain experimentally observed features of the response (Bažant 1967). In concrete, however, the initial anisotropy is negligible, and even the stress-induced anisotropy appears to be insufficient to permit explaining axial splitting fractures in terms of three-dimensional buckling—at least not as the initial triggering mechanism (although after the axial splitting failure of a concrete specimen is initiated, three-dimensional buckling might still play a role in the failure process).

In this study, another idea is advanced. The uniformity-breaking mechanism may be provided by the formation and propagation of a damage (cracking) band exhibiting strong volume dilatancy caused by growth of axial splitting microcracks that are parallel to the direction of compression. In such a band, one can expect an inelastic volume dilatancy to be produced due to high deviatoric stresses. The volume dilatancy must induce transverse tensile stresses in front of the splitting microcracks, which causes them to grow. That does not mean, however, that the bands of axial splitting cracks should grow in the direction of compression; rather these cracks form a band propagating in the inclined direction.

This mechanism is quite different from the tensile fracture mechanism, because generation of the transverse tensile stresses in front of the cracking band by volume dilatancy in the band can be a purely local mechanism that involves no significant stress and strain changes anywhere except rather near the fracture band. Therefore, the basic properties of such fracture, especially the size effect, could be quite different.

As is well known from the studies of nonlinear triaxial behavior of concrete as well as geomaterials, realistic predictions of inelastic volume dilatancy due to deviatoric stresses require a relatively sophisticated nonlinear triaxial constitutive model, covering the postpeak strain softening. Most of the constitutive models previously proposed for concrete work well only for uniaxial and biaxial stresses but not after the peak. We select for the present study the microplane model in which the normal microplane strains are split into volumetric and deviatoric components, as introduced in Bažant and Prat (1988). This model has been shown to represent quite well a very broad range of experimentally observed behavior including various types of triaxial tests, biaxial tests, biaxial and triaxial failure envelopes, softening response, etc. Furthermore, the nonlocal extension of this model has been shown to work well for tensile fracture and represent the observed size effect. A somewhat different type of extension of the previous microplane model, which can also model compression failures, has been developed by Hasegawa and Bažant (internal report, Northwestern University, 1990).

There has been extensive research into micromechanics of compressive failure of various materials (Brockenbrough and Suresh 1987; Ingraffea 1977; Kendall 1978; Miyamoto et al. 1977; Sammis and Ashby 1986; Shetty et al. 1968). Mechanisms such as the propagation of axial cracks from voids or the so-called wing-tip cracks were studied by many researchers. These studies, however, illuminated only some microstructural mechanisms but have not lead to a general macroscopic model capable of furnishing the load-displacement curves and failures states of specimens or structures.

Numerical Modeling of Compression Splitting Fracture

We analyze a rectangular concrete specimen of size 300 × 300 × 540 mm [Figs. 1(*a*) and (*b*)] uniaxially compressed between perfectly rigid platens. The specimen may be imagined to represent the cross section of a wall that is in a plane strain state. The finite element mesh is shown in Fig. 1. The material parameters of the microplane model, as defined in the previous

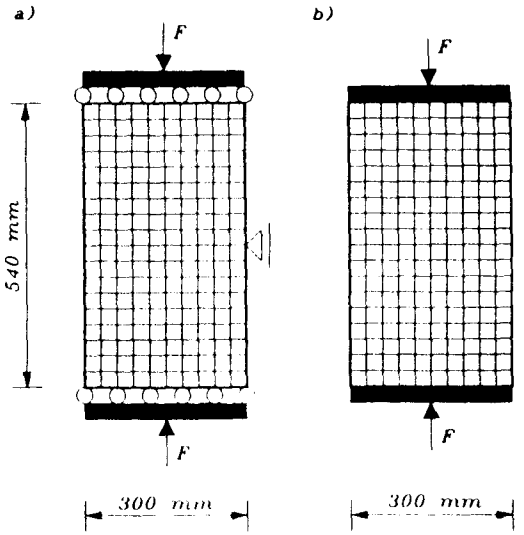

FIG. 1. Specimens Analyzed, with Finite Element Meshes

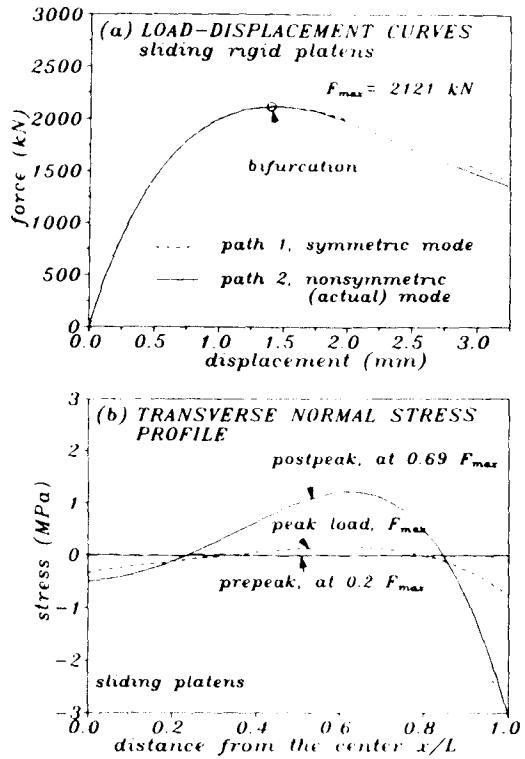

FIG. 2. (*a*) Calculated Curve of Load versus Axial Displacement for Specimens with Sliding Rigid Platens; and (*b*) Calculated Profiles of Transverse Normal Stresses Along Symmetry Axis of Specimen

study by Bažant and Prat (1988), are taken according to that study as: E_0 = 23,500 MPa (initial elastic modulus), and ν = 0.18 (Poisson ratio), a = 0.005, b = 0.043, p = 0.75, q = 2.00, e_1 = 0.00006, e_2 = 0.0015, e_3 = 0.0015, e_4 = 0., m = 1.0, n = 1.0, k = 1.0. Most of these parameters, except e_1, e_2, e_3, e_4, can be considered to have the same value for all concretes, as specified in Bažant and Prat (1988). Based on these parameter values, calculations of the uniaxial stress-strain curve for a single material point yield uniaxial compression strength 17.6 MPa and tensile strength 1.72 MPa. The maximum aggregate size is d_a = 30 mm, and the characteristic length is assumed as $l = 3d_a$.

Compared to the previous microplane model, however, a minor modification has been made; while previously the microplane shear stress and strain vectors were assumed to always be coaxial, presently they are allowed to be noncoaxial. These vectors are split in two components with respect to the rectangular in-plane coordinate axes, whose directions are chosen randomly on each microplane. (This randomness introduces a slight nonsymmetry into the model with respect to the plane of symmetry of the specimen.) The relation between the shear stress and strain components for each component direction is assumed to be the same as that between the shear stress and shear strain in the previous model.

The compression specimens are loaded through perfectly rigid platens and anlayzed both for perfectly sliding (frictionless) platens [Fig. 1(*a*)], and for bonded (nonsliding) platens [Fig. 1(*b*)]. The specimen is loaded in small steps by prescribing axial displacement increments of the top platen in each loading step. To initiate a softening damage band in the direction of compression, there must be some small initial random inhomogeneity, from which the band starts. Therefore we assume that there is a weak zone in the center of the specimen; see the shaded area in Fig. 1. The elastic modulus in the weaker zone is assumed to be 5% less than in the rest of the specimen. Isoparametric four-node quadrilaterals with four integration points are used in the calculations. All the elements are identical and their size is equal to 1/3 of the characteristic length l. For a completely symmetric situation, one may expect symmetry-breaking bifurcations of the response. As we will see, numerical results indicate that this indeed occurs for the case of the sliding boundary (but, curiously, not for the case of the boundary with perfect bond to the rigid platens, called the bonded boundary).

To determine bifurcations and stability, the tangential stiffness matrix K_t is calculated at various states by imposing $q_i = 1$, with all other $q_j = 0$; q_i are all the displacements of the structure ($i,j = 1,2, \ldots n$). Matrix $\mathbf{K}_t$ is usually nonsymmetric. Because of various possible combinations of loading and unloading at various integration points and at various microplanes at each point, there are great many matrices K_t at each stage of loading; each of them corresponding to a different sector of the space of all q_i. However, in similarity to Hill's method of linear comparison solid (Hill 1961, 1962), known from plasticity, the first bifurcation of the loading path can be determined by considering only the K_t matrix for the same unloading-loading combinations as for the previous loading steps. For the first bifurcation, this means considering matrix $K_t = K_t^I$ that is calculated under the assumption that loading occurs for all q_i. Matrix K_t is in general nonsymmetric. Let $\bar{K}_t$ be its symmetric part, i.e., $\bar{K}_t = (K_t + K_t^T)/2$, and let λ_1 and $\hat{\lambda}_1$ be the first (i.e., minimum) eigenvalues of matrices K_t and $\bar{K}_t$. Before the first bifurcation, $\lambda_1 > 0$. At the first bifurcation $\lambda_1 = 0$, and after the first bifurcation, $\lambda_1 < 0$. Stable states are characterized by $\hat{\lambda}_1 > 0$, the limit of stability of the structure is characterized by $\hat{\lambda}_1 = 0$, and unstable states are characterized by $\hat{\lambda}_1 < 0$. The stable path is characterized by $\lambda_1 > 0$, where λ_1 is calculated from K_t for the precise loading-unloading combination for that path. According to Bromwich's theorem known from linear algebra, always $\lambda_1 \leq \hat{\lambda}_1$, i.e., the first bifurcation occurs at or before the onset of instability [for detailed explanations, see section 10.4 in Bažant and Cedolin (1991)].

The mathematical analysis of bifurcation states and postbifurcation paths can be avoided if one introduces small imperfections into the system, provided of course that these imperfections are chosen such that they excite the secondary postbifurcation path. Thus, λ_1 and $\hat{\lambda}_1$ have been calculated only for some states of the perfect system, while generally the imperfection approach has been followed, making the finite element meshes for both types of the boundary conditions slightly asymmetric. This has been done by slightly displacing four interior nodes near the center of the specimen in the lateral direction.

Results of Numerical Analysis

The results of analysis for the case of sliding boundaries are shown in Figs. 2–8. The calculated load-displacement curves for perfectly symmetric

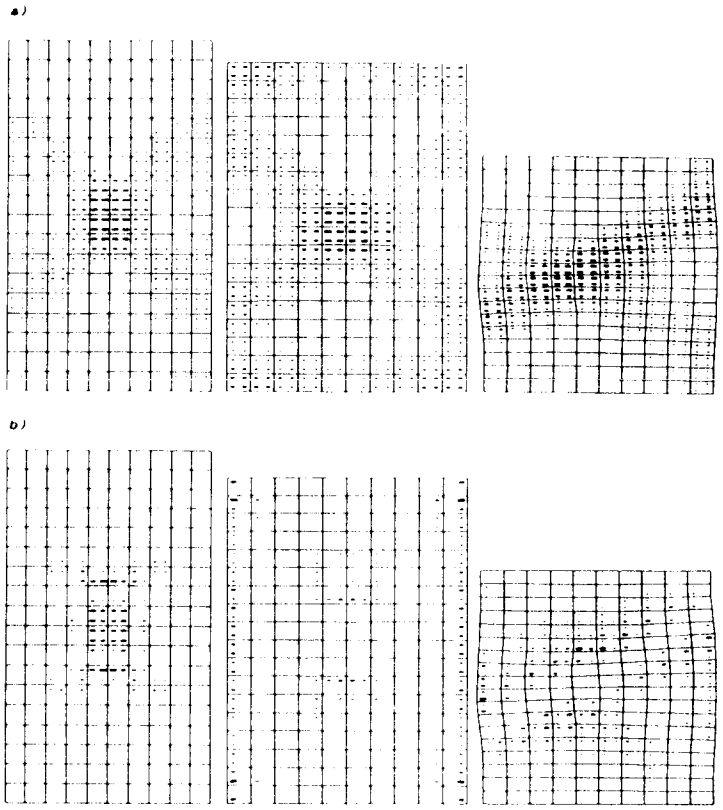

FIG. 3. Deformed Meshes (Exaggerated 50 Times) with Fields of (*a*) Maximum Principal Strains ε_1; and (*b*) Maximum Prinicipal Stresses σ_1 (Tensile Only)—for Sliding Platens (Actual Path), at Prepeak ($0.2F_{max}$), Peak Load (F_{max}), and Postpeak ($0.64F_{max}$). (Size of Rectangles is Proportional to Magnitude and Direction of Their Long Side is ε_1-Direction)

and slightly asymmetric finite element meshes [Fig. 2(*a*)] are visually undistinguishable up to a point that lies slightly beyond the peak-load point. For the perfectly symmetric mesh, a bifurcation occurs at this point, which is revealed by singularity of the tangential stiffness matrix. The bifurcation is caused by a breakdown of symmetry in the specimen response and is a consequence of strain softening of the material. As shown in Bažant (1989a), and Bažant and Cedolin (1991, Chapter 10), for the conditions of displacement control, the path that occurs after the bifurcation point must minimize the second-order work $\delta^2 W = \delta f \delta u/2$; where δu is the prescribed displacement increment, and δf is the force reaction increment at the top of the specimen. As expected, smaller value of $\delta^2 W$ is obtained for the secondary bifurcated path that yields an asymmetric response mode. Consequently, the path that actually occurs must be the symmetry-breaking secondary path. The fact that the primary path is not the actual path is also confirmed by negativeness of the smallest eigenvalue of the tangent stiffness matrix after

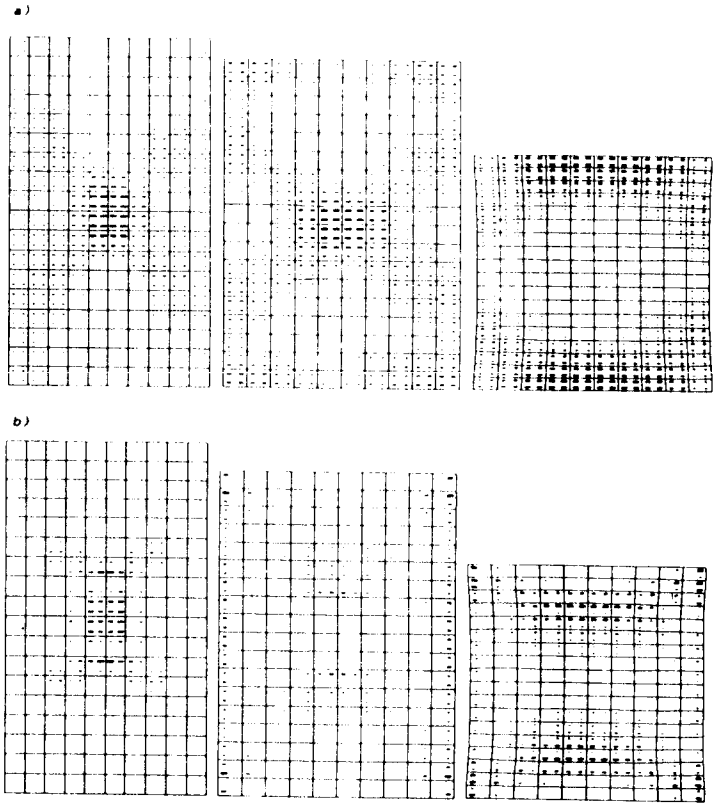

FIG. 4. Same as Fig. 3 but Symmetric Deformation Enforced (Not Actual Path), at Prepeak State ($0.2F_{max}$), Peak Load (F_{max}), and Postpeak State ($0.69F_{max}$)

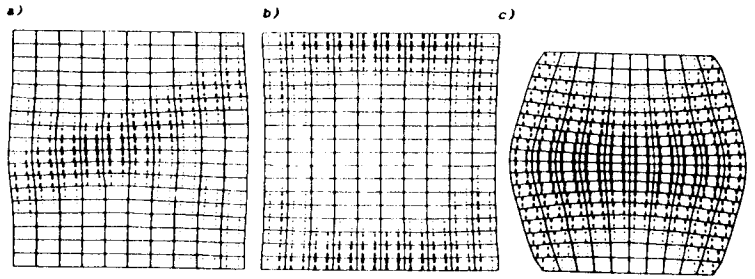

FIG. 5. Cracking Patterns Represented by Fields of Maximum Principal Inelastic Strain ε_1'' (Tensile Only), for (*a*) Sliding Platens (Actual Path); (*b*) Sliding Platens (Symmetric Deformations—Not Actual Path); and (*c*) Bonded Platens (Direction of Rectangles Here is Cracking Direction, Normal to ε_1'')

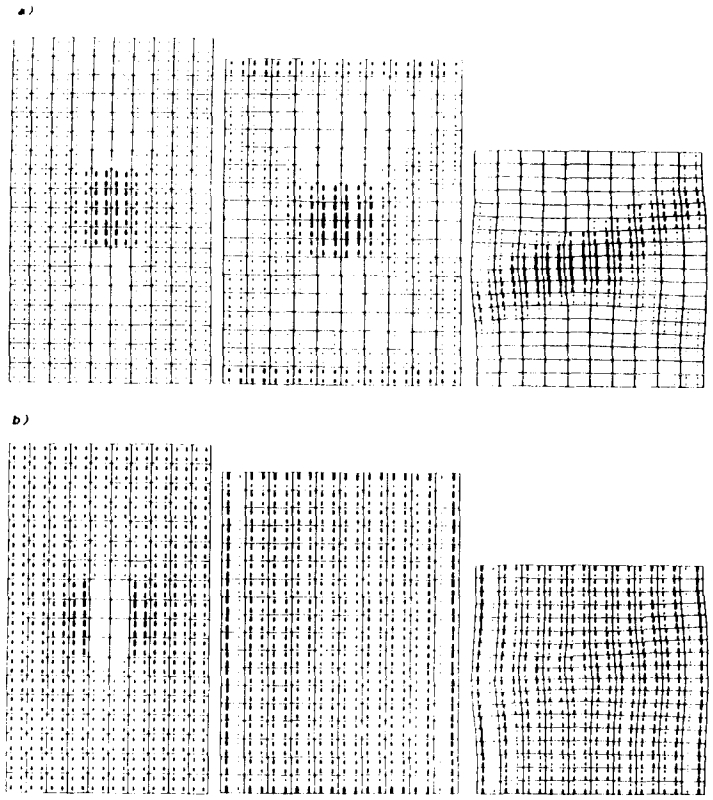

FIG. 6. Deformed Meshes with Fields of (*a*) Minimum Principal Strains ε_3; and (*b*) Minimum Principal Stresses σ_3 (Compressive Only)—for Sliding Platens (Actual Path)

the first bifurcation point, while for the states on the secondary path the smallest eigenvalue remains positive.

Fig. (2*b*) shows the profiles of the transverse normal stress along the specimen axis. Figs. 3(*a*) and (*b*) and 4(*a*) and (*b*) show the magnitudes and directions of the fields of the maximum principal tensile strains and stresses over the deformed specimen at various load levels, for both symmetric and asymmetric response paths. At each integration point at which the maximum principal strain or stress is positive (tension), a solid rectangle is plotted to characterize its magnitude and direction. The size (length) of each rectangle is proportional to the magnitude, and the direction of its longer side shows the principal strain or stress direction. The zones of axial splitting cracks are those in which the maximum principal stresses are negative or small positive [blank zone in Figs. 3(*b*) and 4(*b*)] while at the same time the maximum principal strains are large and positive [zone of large rectangles of Figs. 3(*a*) and 4(*a*)]. As we see, the symmetric path represents pure splitting compression failure while the inclined failure band that develops in the asymmetric path represents a combination of axial splitting with a shear band (it may also be described as a shear band that consists of axial

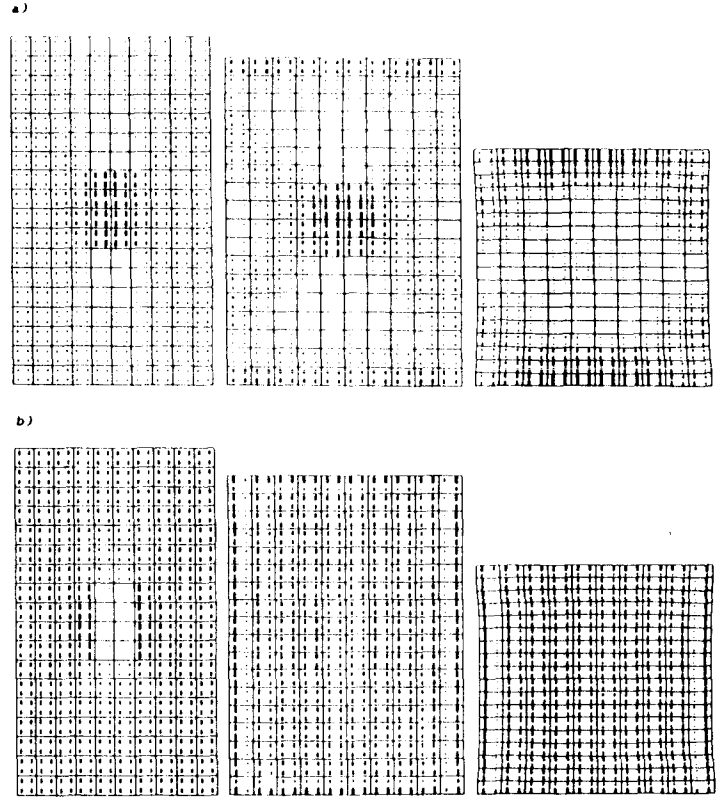

FIG. 7. Same as Fig. 6 but Symmetric Deformation Enforced (Not Actual Path)

splitting cracks). Both modes in Figs. 3(*a*) and 4(*a*) clearly indicate a tendency toward large transverse expansions, which cause vertical (splitting) cracks. We also see that the zone of transverse expansion propagates for the symmetric mode vertically [Fig. 4(*a*)], and for the nonsymmetric mode in an inclined direction [Fig. 3(*a*)]. The driving force of the propagation appears to be the transverse expansion of the crack band front that is caused by deviatoric strains (well captured by the microplane model). Clearly this expansion must produce transverse tensile stresses ahead of the expansion zone and compressive stresses within this zone [Fig. 2(*b*)], causing the splitting cracks to close.

In a smeared, continuum representation, cracking is characterized by the smeared cracking strain ε_{ij}^{cr}. The inelastic strain ε_{ij}'' in general consists of the cracking strain and the plastic strain ε_{ij}^{p}. In the direction of the maximum principal inelastic strain ε_1'', nearly all of it may be assumed to be due to cracking strain ε_1^{cr}, with a negligible contribution from plasticity. Thus, we will assume that $\varepsilon_1^{cr} = \varepsilon_1''$. The inelastic strains are calculated as $\varepsilon_{11}'' = \varepsilon_{11} - (\sigma_{11} - \nu\sigma_{22} - \nu\sigma_{33})/E$, $\varepsilon_{22}'' = \varepsilon_{22} - (\sigma_{22} - \nu\sigma_{11} - \nu\sigma_{33})/E$, and $\varepsilon_{12}'' = \varepsilon_{12} - \sigma_{12}/2G$, where subscripts 1 and 2 refer to the coordinates x_1 and x_2 in the horizontal and vertical directions in Fig. 1; E = Young's elastic

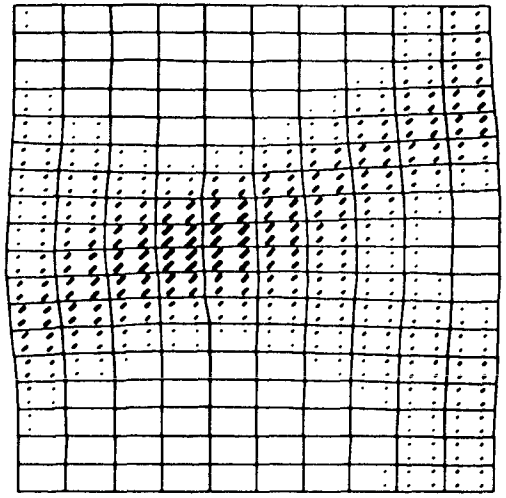

FIG. 8. Field of Maximum Shear Strains for Nonsymmetric (Actual) Deformations, Postpeak, at $0.64F_{max}$ (Size of Each Rectangle Is Proportional to Magnitude, and Longer Side Indicates Stress Direction)

modulus, ν = Poisson ratio, and $G = E/2(1 + \nu)$ = elastic shear modulus. The values of ε_I'' have been calculated from ε_{11}'', ε_{22}'', and ε_{12}'' for all the integration points of all the elements. The distributions of ε_I'' for the nonsymmetric and symmetric deformation mode of a specimen with sliding platens are shown in Figs. 5(*a*) and (*b*), where the size of the rectangles is proportional to the magnitude of ε_I'', while the direction of their longer side is in this case normal (rather than parallel) to the maximum principal direction and indicates the direction of cracking. From Fig. 5(*a*) we see that cracking is essentially vertical everywhere, as expected, and that the zone of major cracking spreads in an inclined direction, thus representing a shear band. Visible cracks occur only in the areas of large ε_I'', while at locations of small ε_I'' there is only invisible microcracking.

At the peak load [Figs. 4(*a*) and (*b*), the cracking front (white area) reaches roughly to the upper and lower quarter of the specimen length. Subsequently, during postpeak softening, the cracking front (white area) propagates still further towards the loading platens. The progress of the cracking front toward the platens is also apparent from Fig. 2(*b*), which shows the distribution of the transverse normal stresses (average value for each finite element) along the specimen axis at various load stages.

Figs. 6(*a*) and (*b*) and (7*a*) and (*b*) further show the field of minimum principal (compressive) strains and stresses, which exists in the region that is blank in Figs. (3*b*) and 4(*b*) and corresponds to the field of maximum principal (tensile) strains shown in Figs. (3*a*) and 4(*a*) (the rectangles are not plotted only for the zones of negative strains or stresses).

Fig. 8 shows the maximum shear strain for the nonsymmetric failure mode. This figure clearly indicates that the inclined bands are really shear bands.

The results of the analysis for the case of nonsliding boundaries are shown in Figs. 5(*c*), and 9–11. The load-displacement curve [Fig. 9(*a*)] exhibits a slightly higher peak load than that in the case of sliding boundaries, while the descending branch is steeper. It is interesting that in this case the re-

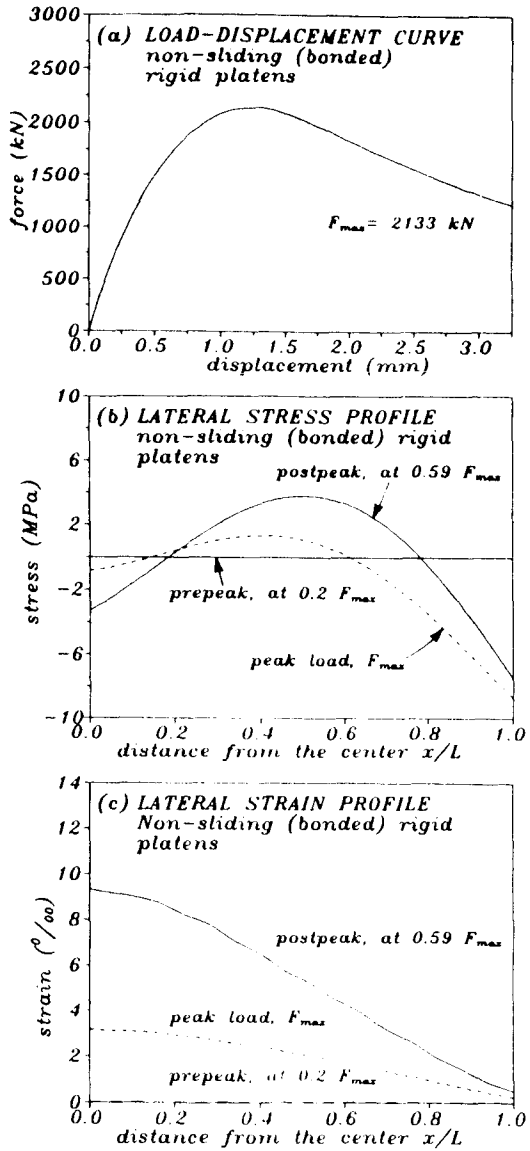

FIG. 9. (a) Load-Displacement Curve for Specimen with Bonded (Nonsliding) Platens, and Profiles of Lateral (*b*) Stress and (c) Strain for Bonded (Nonsliding) Platens

sponse of a symmetric specimen exhibits no bifurcation. This is verified by introducing a slight nonsymmetry into the computational model. The load-displacement curve remains nearly the same, and so does the failure mode for this specimen.

Fig. 5(*c*) shows the distribution of maximum principal cracking strain ε''

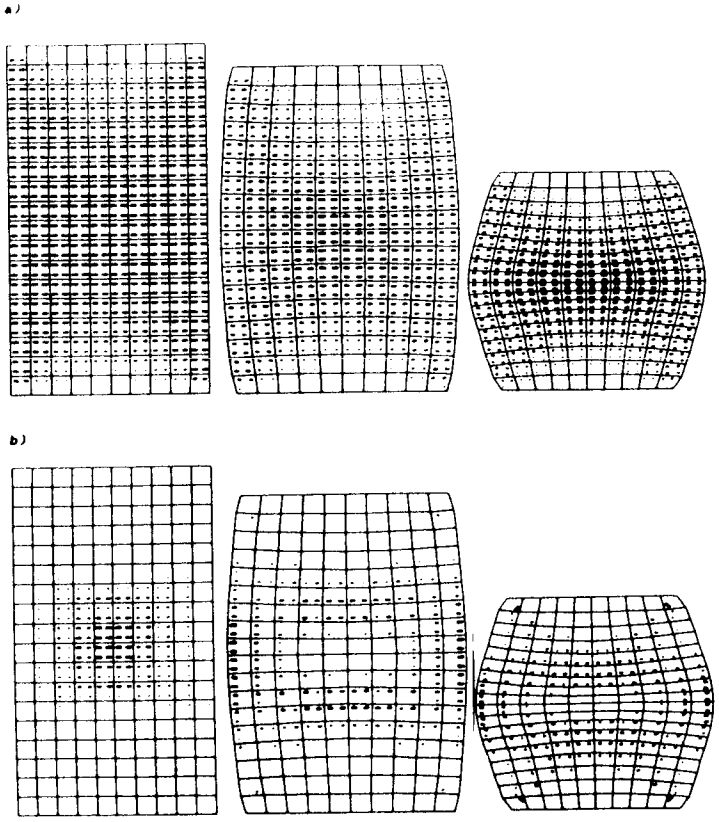

FIG. 10. Deformed Meshes (Exaggerated 50 Times) with Fields of (a) Maximum Principal Strains ε_1; and (b) Maximum Principal Stresses σ_1 (Tensile Only)—for Bonded Platens (Actual Path), at Prepeak ($0.2F_{max}$), Peak Load (F_{max}), and Postpeak ($0.59F_{max}$). (Size of Rectangle is Proportional to Magnitude and Direction of Their Long Side is ε_1-Direction)

[in the same manner as Fig. 5(*a*) and (*b*)]. The cracking starts to propagate vertically from the assumed weak zone at the center of the specimen, moving first towards the loading platens. Then, however, already before reaching the peak-load state, the band of vertical splitting cracks starts to propagate sideways, in two inclined directions. This happens for the present p-value while the cracking front reaches roughly to the top and bottom quarters of the specimen height. The magnitudes and directions of the fields of the maximum and minimum principal stresses and strains at various load levels are shown in Figs. 9–11. Figs. 9(*b*) and 9(*c*) show the distribution of the lateral stresses and strains along the vertical axis at various load stages.

To investigate the size effect, the aforementioned calculations for the case of a perfectly symmetric mesh have been repeated for geometrically similar specimens of three different sizes in the ratio 1:2:4, the smallest specimen having the height $h = 61 = 540$ mm. It is highly interesting, although perhaps not surprising with respect to the knowledge from experiments, that no significant size effect has been detected from the calculated results.

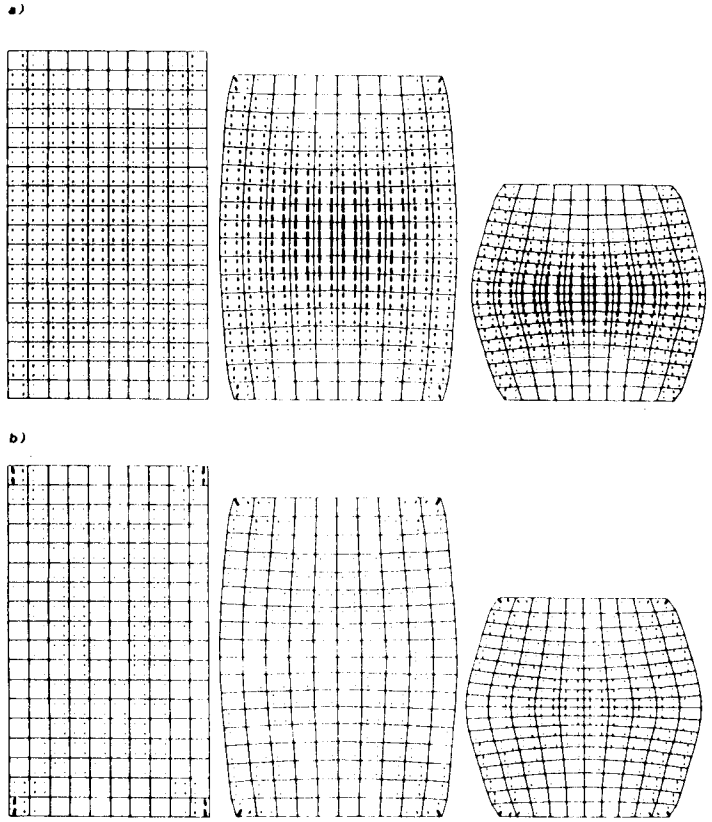

FIG. 11. Deformed Meshes with Fields of (a) Minimum Principal Strains ε_1; and (b) Minimum Principal Stresses σ_1 (Compressive Only)—for Bonded Platens (Actual Path)

that no significant size effect has been detected from the calculated results. [In compression there is, however, the size effect of specimen length on the postpeak softening slope, as shown experimentally by van Mier (1984) and modeled by Bažant (1989b); see also Bažant and Cedolin (1991), section 13.2)

The lack of size effect means that compression fracture cannot be driven by the stored elastic energy that is released globally from the entire specimen. Rather, it must be driven by a local mechanism in a region of a fixed size (depending on l but not on the specimen size) near the fracture front. This mechanism must be approximately independent of the specimen shape and boundaries, and thus involves no significant stress changes farther away from the crack band front. The length of the zone of significant transverse normal stress in Fig. 2(*b*) is approximately constant, independent of the specimen size.

It may also be noted from Fig. 3(*a*) and (*b*) that the tendency toward development of two symmetric inclined failure bands exists at the beginning of the analysis of the perfectly symmetric specimen with sliding boundaries

but is later overridden by the development of an asymmetric shear band. In the specimen with nonsliding (bonded) boundaries, on the other hand, symmetric inclined failure bands (shear bands) tend to develop also, extending toward the specimen corners. The fact that the specimen with nonsliding boundaries does not exhibit any tendency to nonsymmetric failure bands is interesting and contradicts some previous views; this fact is probably due to large transverse normal strains in the middle of the specimen. They apparently override the tendency to nonsymmetric inclined failure bands and enforce symmetric response.

Figs. 12(*a*)–(*c*) show the distribution of the relative volume change ε_V ($\varepsilon_V = \varepsilon_{kk}/3$) at the postpeak state (for both sliding and nonsliding boundaries). The circular dots are plotted only for negative ε_V and their magnitude is proportional to ε_V. It is interesting that, despite large transverse expansions, the volumetric strains are negative almost everywhere, except in the case of the nonsliding boundaries in which only slight positive volumetric strains are detected at the middle of the vertical sides.

Figs. 12(*d*)–(*f*) show the distribution of the inelastic volume change (dilatancy), defined as $\varepsilon_V'' = \varepsilon_V - \sigma_V/3K$ where $\sigma_V = \sigma_{kk}/3$ = mean stress and K = elastic bulk modulus. In contrast to Figs. 12(*a*)–(*c*), the dots are now plotted only for positive ε_V'' and their size is proportional to ε_V''. We clearly see the dilatancy to dominate in the zones of axial splitting cracks or within the shear bands. Thus, the term shear-dilatancy bands appears to be appropriate.

From the calculated strain and stress fields, the cracking pattern of the specimens with sliding and nonsliding boundaries can be reconstructed based on the analysis results shown in Figs. 5(*a*) and (*c*). The spacing of the densely

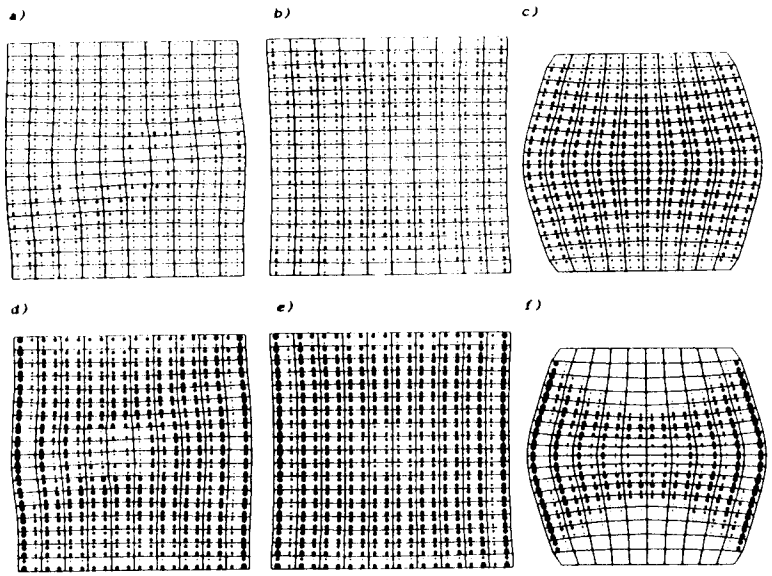

FIG. 12. Postpeak Fields of [(*a*), (*b*), (*c*)] Volumetric Strain ε_V (Negative Only) and [(*d*), (*e*), (*f*)] Inelastic Volumetric Strain (Dilatancy, Positive Only); (*a*), (*b*), (*d*), and (*e*)—Sliding Platens; (*c*) and (*f*)—Bonded Platens; (*a*) and (*d*)—Nonsymmetric (Actual) Path, (*b*) and (*e*)—Symmetric Path (Dot Diameter Is Proportional to ε_V)

distributed cracks cannot be obtained from the constitutive model. No doubt it is governed mainly by the size of the dominant inhomogeneities in the material.

The compression failure was previously investigated by a rather different constitutive model, which was not very realistic for triaxial stress states: a nonlocal version of the Drucker-Prager plasticity model with a degrading yield limit (Droz and Bažant 1988). Like in the present study, it was found that the response path of a perfectly symmetric specimen bifurcates, after which either two crossing inclined shear bands may grow (path 1) or only one band may grow while the other unloads (path 2). The asymmetric path (path 2) was found to be the actual path, for both sliding and nonsliding boundaries, and (in contrast to the present results), the difference between the symmetric and nonsymmetric responses was found more pronounced for the case of bonded platens. Due to a different (and more realistic) constitutive model, which gives a much better representation of inelastic volume dilatancy, the present analysis indicates the nonsymmetric component of the failure mode to occur only for specimens with sliding boundaries.

Conclusions

1. The previously developed nonlocal microplane model with normal microplane strains that are split into deviatoric and volumetric components appears to be capable of modeling axial splitting cracks and shear band failure of quasibrittle materials in compression.
2. The most important characteristic of compression failures in quasibrittle materials may be described in the continuum sense as tensile strain softening in the transverse direction (increase of transverse strain at decreasing transverse stress). In reality, this strain softening is manifested as damage by densely distributed axial splitting cracks. According to the present results, the axial splitting cracks appear to be caused by transverse expansion in the fracture process zone, which puts the region in front of the expansion zone into transverse tension. The axial splitting cracks organize themselves into inclined shear band propagating sideways, rather than in the direction of the cracks.
3. For specimens with perfectly sliding platens, the primary path that corresponds to symmetric deformation bifurcates, and the actual path that occurs corresponds to asymmetric deformation with one dominant inclined failure band. Bifurcation analysis can be skipped and the asymmetric deformation obtained directly if a slight asymmetry is introduced into the computational model. Without such artificial asymmetry the bifurcation is indicated by the vanishing of the smallest eigenvalue of the tangential stiffness matrix of the structure. The postbifurcation states are stable because the smallest eigenvalue of the symmetric part of the tangential stiffness matrix of the structure remains positive (under displacement-controlled loading).
4. For specimens bonded to rigid loading platens, no bifurcation is found and the failure mode involves two symmetric inclined shear bands that consist of smeared axial splitting cracks (transverse expansion with strain softening).
5. Despite large transverse expansion, the relative volume change for all the analyzed cases is negative, except for a small zone at the middle of the vertical sides in a specimen with bonded rigid platens. On the other hand, the inelastic part of the volume change (i.e., dilatancy) is positive over a large part of the specimen. The shear bands represent zones of large inelastic dilatancy, and not

only large shear strains; thus they might be more aptly called "shear-dilatancy" bands (or "shear-expansion" bands).

6. It is most interesting that the present model reveals no appreciable size effect on the nominal stress at maximum load when geometrically similar specimens of different sizes (with the same characteristic length l) are compared. This means that (1) The mechanism that drives the axial splitting must be local, coupled to the width of the shear band, which is about the same for different specimen sizes; and (2) no significant release of stored energy from the specimen as a whole into the cracking front takes place.

7. In contrast to tensile fracture, a successful modeling of compression failures apparently necessitates a constitutive model that gives not only correct shear deformations but also correct transverse expansions and volume dilatancy under complex triaxial stress states. The microplane model appears to satisfy this requirement.

Acknowledgments

Partial financial support for nonlocal analysis was received from the Air Force Office of Scientific Research (under Grant 91-0140 to Northwestern University), and for the underlying fracture studies from the Center for Advanced Cement-Based Materials at Northwestern University. Most of the paper was written during the first writer's sojourn at Lehrstuhl A für Mechanik, Technische Universität München, supported under A. von Humboldt Award of Senior U.S. Scientist.

Appendix. References

Bažant, Z. P. (1967). "Stability of continuum and compression strength." *Bulletin RILEM*, Paris, France, 39, 99–112 (in French).

Bažant, Z. P. (1989a). "Bifurcation and thermodynamic criteria of stable path of structures exhibiting plasticity and damage propagation." *Computational Plasticity* D. R. J. Owen, E. Hinton, and E. Onate, eds., Pineridge Press, Swansea, U.K., 1–25.

Bažant, Z. P., (1989b). "Identification of strain-softening constitutive relation from uniaxial tests by series coupling model for localization." *Cement and Concrete Res.*, 19, 973–977.

Bažant, Z. P., and Cedolin, L. (1991). *Stability of structures: Elastic, inelastic, fracture and damage theories*. Oxford Univ. Press, New York, N.Y.

Bažant, Z. P., and Ožbolt, J. (1990). "Nonlocal microplane model for fracture, damage, and size effect in structures." *J. Engrg. Mech.*, ASCE, 116(11), 2485–2504.

Bažant, Z. P., and Prat, P. C. (1988). "Microplane model for brittle plastic material, I. Theory and II. Verification." *J. Engrg. Mech.*, ASCE, 114, 1672–1702.

Brockenbrough, J. R., and Suresh, S. (1987). "Constitutive behavior of a microcracking brittle solid in cyclic compression." *J. Mech. Phys. Solids*, 356, 721–742.

Droz, P., and Bažant, Z. P. (1988). "Nonlocal analysis of stable states and stable paths of propagation of damage shear bands." *Cracking and damage*, J. Mazars and Z. P. Bažant, eds., Elsevier, London, England, 183–207.

Glucklich, J. (1963). "Fracture of plain concrete." *J. Engrg. Mech. Div.* ASCE, 89(6), 127–138.

Griffith, A. A. (1924). "The theory of rupture." *Proc. 1st Int. Conf. Applied Mechanics*, Delft, The Netherlands, 55–65.

Hill, R. (1961). "Bifurcation and uniqueness in non-linear elastic-plastic solids." *J. Mech. Phys. Solids*, 6, 236–249.

Hill, R. (1962). "Uniqueness criteria and extremum principles in self-adjustment problems in continuum mechanics." *J. Mech. Phys. Solids*, 10, 185–194.

Ingraffea, A. R. (1977). "Discrete fracture propagation in rocks: Laboratory tests and finite element analysis," dissertation presented to the University of Colorado, at Boulder, Colorado, in partial fulfillment of the requirements for the degree of Doctor of Philosophy.

Kendall, K. (1978). "Complexities of compression failure." *Proc. Royal Soc. of London*, A. 361, 245–263.

Lawn, B. R., and Marshal, D. B. (1978). "Indentation fracture and strength degradation in ceramics." *Fracture mechanics of ceramics*, 3, R. C. Bradt, ed., Plenum Press, 205–229.

Miyamoto, H., Fukuda, S., and Kageyama, K. (1977). "Finite element analysis of crack propagation under compression." *Fracture 1977*, Vol. 3, ICF4, Waterloo, Canada, 491–499.

Sammis, C. G., and Ashby, M. F. (1986). "The failure of brittle porous solids under compressive stress state." *Acta Metallurgica*, 34(3), 511–526.

Shetty, D. K., Rosenfield, A. R., and Duckworth, W. H. (1968). "Mixed mode fracture of ceramics in diametral compression." *J. American Ceram. Soc.*, 69(6), 437–443.

van Mier, J. G. M. (1984). "Strain-softening of concrete under multiaxial loading conditions," thesis presented to Eindhoven University of Technology, at Eindhoven, The Netherlands, in partial fulfillment of the degree of Doctor of Philosophy.